Journal of Cleaner Production 274 (2020) 123450

Contents lists available at ScienceDirect

Journal of Cleaner Production

journal homepage: www.elsevier.com/locate/jclepro

Exploring sulfate and metals removal from Andean acid mine drainage using $CaCO_3$-rich residues from agri-food industries and witherite ($BaCO_3$)

Alfonso Larraguibel [a, b, **], Alvaro Navarrete-Calvo [a, b], Sebastián García [b, c], Víctor F. Armijos [d], Manuel A. Caraballo [b, c, *]

[a] Geology Department, University of Chile, Plaza Ercilla 803, Santiago, Chile
[b] Advanced Mining Technology Center, University of Chile, Avda. Tupper 2007, 8370451, Santiago, Chile
[c] Mining Engineering Department, University of Chile, Avda. Tupper 2069, Santiago, Chile
[d] Innovation and Knowledge Department, Sacyr Chile, Isidora Goyenechea 2800, Santiago, Chile

ARTICLE INFO

Article history:
Received 1 February 2020
Received in revised form
4 July 2020
Accepted 25 July 2020
Available online 9 August 2020

Handling Editor: Jiri Jaromir Klemeš

Keywords:
Dispersed alkaline substrate
Malachite
Acid mine drainage
Seashells
Passive treatment system

ABSTRACT

Dispersed alkaline substrate (DAS) is a matured passive remediation technology that has shown very high performances treating acid mine drainages (AMD). However, this remediation approach needs to improve its environmental footprint as well as to ensure almost complete water sulfate removals for longs periods of time. The present study improves the use of witherite ($BaCO_3$) as a reagent on DAS-type treatments to induce highwater sulfate removals in the context of Andean AMD. Also, three $CaCO_3$-rich residues from the agri-food industry were tested as alternatives to the current use of limestone. Two sets of column experiments were developed with various flow rates (1.5–5.4 L/day), net acidities (202 and 404 mg/L as $CaCO_3$ eq.) and reactive agents (calcite, eggshells, seashells and witherite). Seashells were validated as a perfect limestone substitutes on the $CaCO_3$-DAS stages. Malachite was observed, for the first time within these columns, as a mineral phase actively involved in Cu water removal. The $BaCO_3$-DAS columns achieved values under 500 mg/L of sulfate at the output of the system for up to 6 months (initial sulfate concentration ranged 1234–2468 mg/L). Upscaling calculations of the present results support the feasibility of using this technology at a full field scale, especially as a wastewater treatment for abandoned mine sites, although some strategies to reduce witherite costs are recommended.

1. Introduction

Acid mine drainage (AMD) is a specific type of water pollution resulting from its interaction with sulfide minerals (mainly pyrite) at oxidizing environments (Dold, 2014). As a result, this environmental problem is ubiquitously present around the world in mined and un-mined sulfide rich rocks (Jacobs et al., 2014). These drainages are characterized by high metals and sulfate concentrations and low pHs, making them extremely harmful for the environment, causing severe biotic impairment (only extremophile forms of life like bacteria, fungus or algae remain present) and making the waters unsuitable for other human uses (i.e., consumption, agriculture, farming, …) (Skousen et al., 2017; Younger and Wolkersdorfer, 2004; Akcil and Koldas, 2006).

Because of the severity and widespread distribution of this water pollution around the world, a substantial amount of different remediation approaches has been generated during the last three decades (Younger et al., 2002; Ziemkiewicz et al., 2003; Ayora et al., 2013). The most frequently used treatments to remediate high flowrates of AMD are characterized by an intensive use of energy to power the multiple mobile mechanical parts and electronical components of the industrial treatment plants (Johnson and Hallberg, 2005; Kefeni et al., 2017), and for this very reason this approach is typically referred as active treatments. The particular design of an active treatment depends on both the specific water pollution to be treated and the water quality to be achieved at the output of the system. Therefore, a variety of treatments units (e.g.,

* Corresponding author. Advanced Mining Technology Center, University of Chile, Avda. Tupper 2007, 8370451 Santiago, Chile.
** Corresponding author. Geology Department, University of Chile, Plaza Ercilla 803, Santiago, Chile.
E-mail addresses: alfonso.larraguibel@ing.uchile.cl (A. Larraguibel), mcaraballo@ing.uchile.cl (M.A. Caraballo).

https://doi.org/10.1016/j.jclepro.2020.123450
0959-6526/

neutralizing reactors, softening reactors, filtration and/or reverse osmosis) are frequently connected in series to achieve the desired water quality (Johnson and Hallberg, 2005; INAP, 2003). However, a common denominator of most active treatments is the use of a neutralizing step to raise water pH and induce the precipitation of metals, with lime ($Ca(OH)_2$) as the most frequent chemical reagent. Active treatments commonly require high maintenance, high chemical reagents and energy consumptions and highly specialized operators, resulting in significant capital and operational (CAPEX and OPEX) expenditures. Nowadays, they are used primarily in active mine sites (Johnson and Hallberg, 2005).

On the other hand, there are the so-called passive treatments that use a different approach to treat AMD with a minimal or none use of electrical energy. Those treatment technologies are designed to favor the gravitational flow of the AMD through one or more different substrates and/or steps designed to remove metals and/or sulfate and to increase water pH at the same time. They commonly require important expenditures in the initial construction phase (land removal and civil-engineering-type construction) but with a low maintenance, no energy consumptions and without needing highly specialized operators during the operation of the plant, (high CAPEX but low OPEX). The results are cheaper and more environmentally friendly options if compared with active treatments (Skousen et al., 2017; Johnson and Hallberg, 2005; Gazea et al., 1996). However, as a downside, they use to have some limitations regarding the metals and sulfate concentrations of the inflowing AMD and substantial limitations considering AMD inflow rates (i.e., inflow rates are typically lower than 50 L/s, depending on the water chemistry) (Ziemkiewicz et al., 2003; Ayora et al., 2013; Skousen and Ziemkiewicz, 2005). Passive treatments can also be subdivided in two big categories: biogeochemical- (e.g., vertical flow reactors or aerobic and anaerobic wetlands) or geochemical-based systems (e.g., anoxic limestone drainage or limestone permeable barriers), and different hybrid options combining both of them (Skousen et al., 2017; Sheoran A. and Sheoran V. 2006). Passive treatments systems may face several specific problems depending on their individual design and geochemical or biogeochemical approach. Notwithstanding, most of these treatments frequently suffer from two common problems: clogging (progressively reducing the flowrate that the system can receive) and reactive material passivation (the reactive material get isolated from the AMD by a cover of precipitates and loses its neutralizing capacity) (Ayora et al., 2013; Simón et al., 2005; Rose et al., 2004).

On an effort to overcome the frequent clogging and passivation issues observed on most traditional AMD passive treatment systems, the concept of Dispersed Alkaline Substrate (DAS) was first introduced in 2006 (Rötting et al., 2006a, 2006b). DAS consists on a mixture of a coarse-grained inert material (to prevent clogging problems by the generation of a high porosity substrate) and a fine-grained reactive material (to minimize passivation by enhancing the reactive material dissolution rate) (Rötting et al., 2008a). This treatment technology has been optimized and improved for more than a decade using mostly AMDs from the Iberian Pyrite Belt (IPB, SW Spain) (Ayora et al., 2013; Caraballo et al., 2009, 2011; Macías et al., 2012; Torres et al., 2018) but also from other countries around the world like Ecuador (Delgado et al., 2019) and Canada (Rakotonimaro et al., 2016, 2018). Those polluted waters are characterized by very high to extreme metal and sulfate concentrations and low to very low pH values (Table 1, input waters). Historical operational conditions and performances of the main DAS-type treatment systems (i.e., laboratory column experiments, pilot plants and field full scale treatment systems) has been summarized in Table 1 in order to identify the strengths and weakness of this mature technology. Most laboratory and field experiments until 2018 were based on different combinations of operational units using limestone sand ($CaCO_3$) and/or periclase dust (MgO) as reagents to increase water pH. Typically, limestone dissolution increases water pH around 6 and induces the removal of trivalent metals by the precipitation of schwertmannite ($Fe_8O_8(OH)_6SO_4 * 5H_2O$) and hydrobasaluminite ($Al_4(SO_4)(OH)_{10} * 36H_2O$); whereas periclase dissolution generates water pHs higher than 8.5 inducing the precipitation of divalent metals like zinc (Zn^{2+}), manganese (Mn^{2+}), nickel (Ni^{2+}), cadmium (Cd^{2+}) or cobalt (Co^{2+}) (Table 1). Because the well-known geochemical and mineralogical processes governing trivalent and divalent metals removal (as well as some others metals and metalloids adsorption and/or co-precipitation) have been extensively discussed in previous works (i.e., the substantial bibliography on Table 1), it was decided not to repeat them in the present study and the reader is referred to the previous bibliography for detailed information."

Input and output net acidity (as mg/L of $CaCO_3$) can be used to evaluate the system remediation performance since this parameter is calculated taking into consideration the five most relevant elements controlling the AMDs hydrochemistry (i.e., aluminum Al, copper Cu, iron Fe, Zn and Mn) as well as water pH and alkalinity values. All limestone- and/or periclase-based DAS treatment systems achieved very good acidity removals, being able to reduce water net acidities from values in the range of 1500–5000 mg/L as $CaCO_3$eq. to net acidities at the systems outputs on the range of 0–900 mg/L as $CaCO_3$eq. (depending on the specific experiment performance, Table 1). It is important to highlight that the most recent experiences were able to optimize the system performance and obtain net acidity values at the output of the systems close to 0 mg/L as $CaCO_3$ eq. (i.e., experiences from 2012 to 2018, Table 1). However, all those treatments were unable to significantly reduce sulfate water concentrations, achieving sulfate removals on the range of 0%–40% comparing input and output concentrations (Table 1).

Sulfate upper limit concentrations in water quality guidelines for irrigation or for drinking depend on each country environmental legislation but typical values are on the ranges of 150–1000 mg/L and 250–500 mg/L, respectively (Valenzuela, 2019); whereas AMD waters, at the IPB, treated by limestone- or periclase-based DAS treatments systematically show water sulfate concentrations higher than 3000 mg/L (Table 1).

To tackle the sulfate problem, witherite ($BaCO_3$) was recently tested at laboratory scale as a possible new alkaline reagent substituting limestone or periclase (Torres et al., 2018). Witherite dissolution induces sulfate precipitation as barite ($BaSO_4$) according to the following reaction:

$$Ca^{2+}_{(aq)} + SO_4^{2-}{}_{(aq)} + BaCO_{3(s)} \rightarrow BaSO_{4(s)} + CaCO_{3(s)} \quad (1)$$

Witherite dissolution also increase AMD pH to values around 7 or 8 with the concomitant precipitation of any remnant trivalent metals in solution as well as some divalent metals too (Torres et al., 2018). This recent experiment showed promising results, inducing almost complete sulfate removal and complete net acidity removal (Table 1). However, this exploratory experiment only last one month and a half, used a very low inflow rate (0.4 L/day) and was tested at extreme net acidity conditions (5000 mg/L as $CaCO_3$). Consequently, the obtained results should not be applied directly to other realities characterized by higher flowrates and lower acidities (like the one tested on the present study). Even more importantly, the shortness of the experiment discourages to extrapolate results to operation times longer than a couple of months.

In addition, a recent life cycle assessment study performed on the field full scale DAS passive treatment at Mina Concepción, SW Spain (Martínez et al., 2018), revealed that the use of limestone from a quarry had a substantial impact on its carbon and ecological

Table 1
Historical operational conditions and performance of DAS-type treatment systems.

Location			Monte Romero	Monte Romero	Monte Romero	Shillbottle	Mina Esperanza	Monte Romero	Monte Romero	Almagrera	Poderosa Mine	Mina Concepcion
Experiment Scale			Lab columns	Pilot plant	Pilot plant	Lab columns	Field full scale	Field Pilot plant	Lab columns	Lab columns	Lab columns	Field full scale
Input mean values	pH		2.80	3.30	3.08	3.90	2.65	3.58	2.70	2.60	2.40	2.70
	Al	(mg/L)	106	75	117	200	147	80	128	251	532	119
	Fe		250	315	358	5	900	260	161	744	1052	286
	Zn		365	310	388	102	26	350	431	976	0.06	20
	Mn		22	20	19	77	5	13.50	18	467	0	N/A
	Cu		3.30	1.50	10	N/A	18	2.70	7	165	0.10	N/A
	SO_4^{2-}		3510	3200	3640	N/A	3900	3430	3500	11700	7532	N/A
	Net Acidity	(mg/L of $CaCO_3$)	1727	1500	2450	1500	2500	1609	1800	5000	5000	1300
Output mean values	pH		6.50	6	5.90	9.50	5.70	9.80	6.80	7.50	7.60	7.20
	Al	(mg/L)	2	5.25	3.40	50	2	<0.2	0.26	0	0.10	dl
	Fe		2	237	83	0	600	<0.2	0	0	0.08	25
	Zn		350	294	279	20	15	<0.05	7.84	1.70	0	dl
	Mn		22	20	17	45	3	<0.2	3.38	14.50	0	N/A
	Cu		0.50	0.02	0.20	N/A	0.50	<0.01	0.03	0.05	0	N/A
	SO_4^{2-}		3500	3200	3500	N/A	3500	2800	3600	14400	22	N/A
	Net Acidity	(mg/L of $CaCO_3$)	500	630	632	400	900	0	20	30	0	50
Flow rate	(L/day)		0.14–1			1.50			1	1	0.40	
	(L/min)			1	1			1				
	(L/s)						0.50					0.80
Residence Time	(hours)		31–168	24	24 (Lim), 10 (Per)	12	54	36 (Lim), 12 (Per)	17	17	30	70–160
Duration	(months)		16	11	9	3	20	6	4.5	4.5	1.5	12
Reactive materials			Lim.	Lim.	Lim. & Per.	Per.	Lim.	Lim. & Per.	Lim. & Per.	Lim. & Per.	Lim. & With.	Lim. & Per.
References			Rötting et al. (2008b)	Rötting (2008a)	Caraballo et al. (2009)	Caraballo et al. (2010)	Caraballo et al. (2011)	Macías et al. (2012)	Ayora et al. (2016)	Ayora et al. (2016)	Torres et al. (2018)	Martinez et al., 2018

All locations are in the Iberian Pyrite Belt, SW Spain except for Shillbottle that is in NE England.
Lim. = Limestone ($CaCO_3$); Per. = Periclase (MgO); With. = Witherite ($BaCO_3$).
N/A: Not Analyzed or Not Available, dl: Detection Limit.
Net acidity calculated as follows when not directly available: $50.045(3C_{Al}+2C_{Fe}+2C_{Mn}+2C_{Zn}+2C_{Cu}+10^{-pH})$-alk. C_X: molar concentrations. Modified from Rötting et al. (2008a) to consider Cu.

footprint. This is due not only to the typical long distances from limestone quarries to mineralized regions where AMD treatments use to be needed, but also from the mining operation at the quarry. On this respect, the reuse of alternative by-product or residues (instead of mining raw materials) should be encouraged.

For instance, seashells are being used to substitute other alkaline materials in very different applications like aggregate in plain concrete (Martinez-Garcia et al., 2017, 2019) or adsorbent in AMD treatments (Bavandpour et al., 2018). Bivalve mollusks represent almost 10% of the world's total fishery production, being 26% of the entire volume (Martinez-Garcia et al., 2019). China is by far the leading producer of bivalve mollusks (10.35 million tons in 2015), followed by far by Japan (819,131 tons in 2010), the United States (676,755 tons), the Republic of Korea (418,608 tons), Thailand (285,625 tons), France (216,811 tons) and Spain (206,003 tons). Other main bivalve-producing countries are Canada, Chile, Italy and New Zealand (FAO, 2018). Regarding eggshell availability, China (the biggest world consumer) and Chile (a small world consumer) consumed roughly 26.4 million tons and 175,000 tons of eggs in 2013 (FAOSTAT). In other words, they generated 2.9 million tons and 19,000 tons of eggshells (considering that eggshells typically represent a 11% of the egg's total weight). Therein, these residues from the agri-food industry could be considered as worldwide distributed and available alkaline replacement.

Also, it is important to consider that all experiments, but the one in 2010 using the AMD from Shillbottle (UK), were performed using AMDs with very high to extreme metal and sulfate contents and the applicability and performance of this technology at lower metal and sulfate concentrations have not been properly studied (Table 1). These AMDs with lower metal and sulfate concentrations are very typical in many mining regions (e.g., porphyry copper deposits, coal deposits, etc.) around the world that could benefit from the implementation of an optimized DAS technology.

The main scopes of the present study are:1) to investigate different options of potentially more sustainable alkaline materials to replace limestone from quarries, 2) to optimize the best sequence of DAS passive treatment steps to treat AMDs with low to medium acidity (<500 mg/L as $CaCO_3$ eq.) and sulfate (<2000 mg/L) contents if compared with previous experiences (Table 1), and 3) to evaluate the use of witherite to remove variable sulfate loads during periods of treatments significantly longer (i.e., higher than half a year) than the forty days used in the only previous study.

2. Materials and methods

2.1. Chilean and Argentinian AMDs as possible low acidity AMD proxies

As mentioned on the introduction section, DAS passive treatment technology has been successfully used to remove di- and trivalent cations from highly polluted AMDs, but its performance on less concentrated AMDs is still pending. Although an efficient and positive applicability of this technology to less polluted waters can be anticipated, its specific implementation is not straightforward

because a few operational parameters must be optimized and its working ranges defined (i.e., residence time, flowrate that can be treated, metal removal efficiency and duration of the reactive material prior to its passivation or its total consumption). On this respect, it was decided to perform an exploratory bibliographic study of reported AMD waters in the Andes (mostly in Chile and Argentina) to obtain a broad picture of the type of low to medium AMD polluted waters developed on this geological setting. In this part of the Andes, the mine industry is heavily focused on Cu extraction and the most common mineral deposits (and residues) include porphyry copper, iron oxide-copper-gold ore deposits (IOCG) and/or iron oxide-apatite ore deposits (IOA), and Strata-bound (Camus and Dilles, 2001; Barra et al., 2017).

In an attempt to characterize AMD flows in Chilean and Argentinean Andes, 296 samples analyses from 32 different field sites were gathered on a database (Table S1, Supplementary Information). The statistical distribution of the samples and the main statistics are shown in Table S1. The original synthetic AMD (AMD 1x, Fig. 1) used in the lab experiments was created to reproduce the water chemistry of a real sample with a net acidity value close to percentile 75 of the generated database (line 171 highlighted on green on Table S1, Supplementary Information). By doubling the concentrations of the original synthetic AMD (AMD 2x, Fig. 1), a net acidity of 404 mg/L as $CaCO_3$eq. was obtained. This new synthetic AMD has a net acidity value close to percentile 90 of the created database of Andean AMDs from Chile and Argentina. Therefore, the present lab experiments will potentially have direct application to most AMDs in our database.

2.2. Experimental design

To achieve the main goals of the present study, a sequence of two different sets of laboratory experiments were designed and implemented ($CaCO_3$-DASand $CaCO_3$-DAS + $BaCO_3$-DAS Experiments in Fig. 1).

During the first experiment, four different calcium carbonate ($CaCO_3$) reagents were tested to evaluate the possible substitution of commercial limestone (traditionally used in all previous field and laboratory DAS studies and obtained from the closest available quarries) by a potentially more sustainable material (i.e., an industrial residue that could be reused and re-conceived as a by-product rather than as a residue). Limestone was bought at a local supplier while eggshells and seashells were acquired (as waste products, no cost) in local poultry and seafood local markets. All materials were hand crushed using an agate mill and sieved under 4 mm. At the same time, the DAS system performance treating an Andean AMD with moderate metals and sulfate concentrations were tested. All the columns were fed for 100 days using the synthetic AMD previously mentioned (Table A1) and a flow rate of 1.5 L/day. This flowrate was selected to obtain a water residence time within the columns around 48 h to favor an optimal operation of the DAS technology, and it was done following the recommendations of a previous study that discussed in detail the optimal working conditions for this type of technology (Ayora et al., 2013). All columns had 50% porosity and a water residence time of 48 h. Reactive material to wood shavings volumetric ratio was 1–4 within the calcite-DAS and clams shells-DAS columns and 1 to 5 within the mussel shells-DAS and eggs shells-DAS columns. Notice that all the columns on this and the following experiments are followed by a decantation/reaction pond, which are designed to ensure the needed time for the water to equilibrate and complete the mineral precipitation reactions involved in the water treatment. Additional details about the columns and decantation ponds setups and construction can be found in the supplementary information (Fig. A1 and A.2, Appendix).

The second experiment was focused on the assessment of different operational parameters affecting sulfate removal using $BaCO_3$-DAS columns on long term experiments. On this respect, AMDs with two different concentrations (x and 2x, Fig. 1 and Table A1) were fed to two different columns using two different

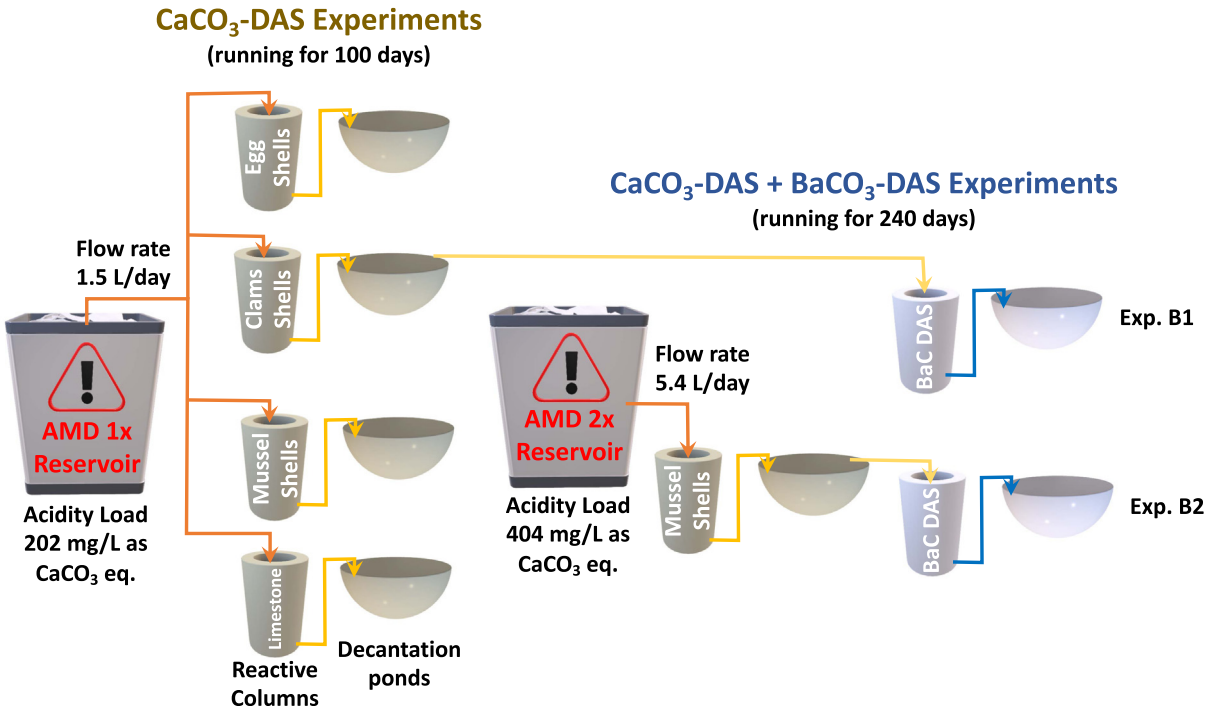

Fig. 1. Experimental design showing the three different experimental setups implemented. The composition of the AMD (mark as x on the graphic) is shown in detail on Table A1 (Appendix). This composition is multiplied by 2 to generate the second AMD reservoir.

inflow rates (1.5 and 5.4 L/day, Table 2). These flowrates were selected to test the effect of high versus low residence times within the columns (48 vs 13.5 h), as well as to study $BaCO_3$-DAS columns performance under two different sulfate loads (i.e., 1.9 and 13.3 g/day). This last experiment was maintained for 8 months to clearly evaluate the system performance during long periods of time.

2.3. Sampling and analysis

Water samples were collected (using lateral sampling ports as well as input and output waters) on a monthly base (or shorter) during the operation time of the different experiments. Filtered samples (filter pore size of 0.45 μm) were acidified with HNO_3 until reaching a pH value close to 1 and stored at the refrigerator at 4 °C until analysis. The chemical analyses were performed by ICP-MS and ICP-OES at external analytical company (i.e., Bureau Veritas/Acmelabs) using a commercial analytical package (i.e., ICP-MS S0200 analysis for natural waters). Additional details about the analytical method can be found in the supplementary information (Appendix A). The detection limits achieved are lower than the regulatory limits proposed by the World Health Organization (WHO, 2008) and the US Environmental Protection Agency (USEPA, 2017). Specific values for these limits are shown in Figure A3 (Appendix).

Physicochemical parameters such as pH, redox potential (Eh), dissolved oxygen (OD) and electric conductivity (EC) were measured using a Thermo Orion Star A329 portable meter, with the following electrodes: For pH Orion 8107UMMD, for ORP measurements Orion 9179BN, for EC Orion 013010MD and for OD Orion 087003. The calibrations solutions used were: Orion pH buffers 910104 (pH 4.01), 910107 (pH 7), 910110 (pH 10.01), ORP standard Orion 967961, EC standards Orion 011007 and Orion 011006. All electrodes were properly calibrated before each measurement campaign.

Solid samples were taken at the end of each experiment, every 4 cm in the upper segment of the substrate and every 6 cm afterwards. An additional sample for each column was taken on the surface (5 mm). The samples were oven-dried (Oven Memmert UN-110) at 30 °C for 3–4 days, milled using an agate mortar and pistil and finally then sieved under 75 μm.

The semi-quantitative mineralogical analyses of the solid samples were obtained using powder X-ray diffraction (XRD) of randomly oriented samples on Bruker D5005 X-ray diffractometer with CuKα radiation. Diffractometer settings were: 40 kV, 30 mA and a scan range of 10–63° 2θ, 0.02° 2θ step size, and 5 s counting time per step. The obtained diffractograms were analyzed using the software XPowderX® and PDF2 database (Fig. 3 and Figures A4 and A.5 on the Appendix). Fluorite was added to the samples as internal standard to correct any possible drifting of the diffractograms and to improve the calculations of the mineral's concentrations. More detail about the specific analysis procedure are offered in the Appendix.

Electron microscopy images and chemical analyses by energy dispersive spectroscopy were obtained with a SEM-EDS FEI Quanta 250. Samples were analyzed using three different detectors: ETD (Everhart Thornley detector), BSED (Backscattered electro detector) and EDX (Energy dispersive x-ray). The instrument was operated using a Voltage range of 10kv to 30kv.The images were processed using the Quanta 250 interface whereas the EDX analysis were studied using the software INCA®.

2.4. Hydrogeochemical model

The geochemical model was implemented using the open source geochemical software (PHREEQC) which is a powerful reaction-based software with a long tradition in the fields of mining and environmental engineering studies (Parkhurst and Appelo, 2013). Detailed explanations of the conceptual geochemical models used as well as the specific chemical reactions, kinetic equations, mineral equilibrium phases, and cells dynamic characteristics during the reactive transport model are offered in the Supplementary Information (Tables A2, A3 and A4).

3. Results and discussion

3.1. Assessment of $CaCO_3$ rich residues from agri-food industries treating an Andean AMD with intermediate metals and sulfate concentrations

As previously mentioned, the first experiment was designed to evaluate: 1) the possible substitution of commercial limestone by a potentially more sustainable material and, 2) the DAS system performance when treating an Andean AMD with moderate metals and sulfate concentrations. Taking into consideration the singularities of the Chilean geography and its industrial matrix, it was decided to test two different types of seashells (clams and mussels shells) as well as eggshells. These materials are very common residues from the Chilean agri-food industries that can be easily found in big amounts on various locations along the country.

As can be observed in Table 3 all experiments showed a very similar performance, achieving almost complete removal of all trivalent metals (i.e., Fe and Al) as well as very high removals for Cu and Zn. The concentrations accomplished by these four elements are under the limits proposed by the World Health Organization (WHO, 2008) and the US Environmental Protection Agency (USEPA, 2017). On the other hand, no significant removal of Mn and sulfate was achieved and their concentrations in the outflowing waters are over the limits proposed by the WHO and the USEPA. Regarding final water pH only small differences were observed, ranging all the experiments between 6.8 and 7.3. So, if the performance of each different reagent is evaluated in terms of metal removal and pH increase, all of them are equally efficient and any of them could potentially be used as neutralizing agent during the $CaCO_3$-DAS step of the passive treatment. However, subtle slower dissolution

Table 2
Main operational conditions of the different columns setups in the experiments including a $BaCO_3$-DAS step.

	Net acidity (mg/L of $CaCO_3$)[a]	SO_4^{2-} (mg/L)	Flow rate (L/day)	SO_4^{2-} load (g/day)	Acid load[b]	Columns residence time (h)	Total duration (months)	Columns reactive materials	Reactive/inert material proportions
Experiment B.1	202	1234	1.50	1.90	53.86	48	8[c]	Clams shells →Witherite	16/84 (v/v) 1/1 (w/w)
Experiment B.2	404	2468	5.40	13.30	387.84	13.50	8	Mussels shells →Witherite	20/80 (v/v) 2/1 (w/w)

[a] Net Acidity = $50.045(3C_{Al}+2C_{Fe}+2C_{Mn}+2C_{Zn}+2C_{Cu}+10^{-pH})$-alk. C_X: molar concentrations. Modified from Rötting et al. (2008a) to consider Cu.
[b] Calculated as (flow rate*net acidity)/(1000*horizontal treatment area).
[c] It is important to keep in mind that the $CaCO_3$-DAS columns have an extra 100 days in these experiments.

Table 3
Mean output water quality parameters from the 4 experiments performed to test different $CaCO_3$ reagents. The values recommended by the World health Organization (WHO, 2008) and the US environmental Protection Agency (USEPA, 2017) are also listed as references.

Reagent	pH	Fe (mg/L)	Al (mg/L)	Cu (mg/L)	Mn (mg/L)	Zn (mg/L)	SO_4^{2-} (mg/L)	Net acidity (mg/L of $CaCO_3$)[a]
Limestone	6.81 ± 0.08	0.125 ± 0.11	0.03 ± 0.01	0.015 ± 0.01	7.24 ± 0.43	0.99 ± 0.50	1179 ± 148	14.91 ± 1.36
Mussels Shells	7.34 ± 0.07	0.1 ± 0.14	0.03 ± 0.01	0.01 ± 0.01	6.63 ± 1.13	0.91 ± 0.66	1281 ± 336	13.89 ± 2.69
Clams Shells	7.34 ± 0.02	0.13 ± 0.16	0.03 ± 0.01	0.01 ± 0.01	5.86 ± 1.42	0.81 ± 0.33	1242 ± 293	12.38 ± 2.75
Egg Shells	7.11 ± 0.07	0.11 ± 0.11	0.02 ± 0.01	0.01 ± 0.01	6.99 ± 0.56	0.14 ± 0.04	1328 ± 231	13.33 ± 1.18
WHO-USEPA		0.30	0.10	2	0.05	5	250	

The values after the ± symbols correspond to the standard deviation of the mean values.
[a] Net Acidity = $50.045(3C_{Al}+2C_{Fe}+2C_{Mn}+2C_{Zn}+2C_{Cu}+10^{-pH})$-alk. C_X: molar concentrations. Modified from Rötting et al. (2008a) to consider Cu.

kinetics and lower final pHs can be observed if limestone and eggshells results are compared with the ones obtained for seashells (clams and mussels, Fig. A.6, Appendix). For all these reasons, it was decided to select seashells as the optimum $CaCO_3$ reagent to be used in the following experiments.

The detailed geochemistry controlling Fe and Al precipitation down the column's profiles (Fig.A.6, Appendix) showed the same trends confirmed in many previous studies (i.e., an upper iron precipitation front controlled by schwertmannite followed by an aluminum precipitation front controlled by hydrobasaluminite, Caraballo et al., 2009). Therefore, it will not be discussed again on this work. However, the new AMD compositions used on the present experiments, more specifically the different ratios between dissolved elements and particularly the low Al/Cu ratio (Table S6, Supplementary Information), induced a geochemical trend for Cu never observed before. This new Cu behavior was almost identical regardless the reactive material employed in the $CaCO_3$-DAS columns. Because of that and to avoid unnecessary redundant information, the following discussion will be focused just on the evolution of the geochemical profile of one selected column. To this end, the first column on experiment B.2 (Fig. 1) was selected because the higher Al and Cu load used in this experiment could allow the better development of two differentiated precipitation fronts for these two elements.

Previous studies have shown that copper precipitation typically mimics the precipitation profile showed by aluminum within the limestone-DAS columns (Ayora et al., 2013; Caraballo et al., 2009). This coupled behavior has been interpreted as Cu co-precipitation and/or sorption in hydrobasaluminite (Caraballo et al., 2009). However, the profiles obtained in the present experiments cannot be exclusively explained by these processes, because sometimes, Cu total removal is obtained deeper in the column profile and after complete Al removal is achieved (Fig. 2A). Additionally, the results of a geochemical model perform to this mussel shells-DAS column anticipate the formation of a Cu precipitation front (made by malachite, $Cu_2CO_3(OH)_2$) right downward the hydrobasaluminite precipitation front (Fig. 2B).

To confirm or deny the precipitation of malachite within the $CaCO_3$-DAS columns (as well as the presence of other mineral phases), several mineralogical analyses were performed (Fig. 3). Before that, a visual inspection of the DAS material during the solid sampling campaign revealed the expected "colored precipitation zone", showing the typical upper orange-reddish zone approximately from 0 to 5 cm depth (and made by precipitated schwertmannite) followed by a whitish zone roughly from 5 to 15 cm depth (made by hydrobasaluminite precipitates). A picture of the column just before the solid sampling campaign is shown in Figure A.7 (Appendix). If some solid samples from the deeper section of the column are looked closely, small particles (shell and wood shaving pieces) coated with a green mineral can be observed (Fig. A.8, Appendix). These green crystals were separated from the main grain, and fizziness was observed when they were put in contact with a drop of 10% HCl (the expected reaction for malachite).

As in most previous studies, the XRD study of the remaining $CaCO_3$-DAS is characterized by an upper section (approximately down to 15–20 cm depth in this experiment) where the alkaline reagent (i.e., aragonite, $CaCO_3$) has been consumed and the only clearly discernible XRD signals (Fig. 3A) correspond to gypsum ($CaSO_4 \cdot 5H_2O$). Also, as usual, the diffractogram showed the typical high background and/or noise due to the presence of a big amount of very poorly crystalline phases like schwertmannite and hydrobasaluminite. However, three very subtle peaks corresponding to malachite were identified on samples at 8–14 cm and 14–20 cm deep (Fig. 3A). The semiquantitative study performed to this sample is in accordance with the previous visual observations and the expected amount of malachite in both samples should be lower than 1% (Fig. 3B). Finally, the presence of malachite was also suggested by the data obtained using electron microscopy, where single particles made by Cu, C and O (detected by EDS) were observed (Fig. 3C).

The most plausible reasons behind the precipitation, for the first time, of malachite in $CaCO_3$-DAS type columns are: 1) the significantly low Al/Cu ratio in the AMD used in the present experiments (Table A.5) and 2) the higher alkalinity achieved in these experiments (around 300 mg/L as $CaCO_3$) comparing with other previous experiments (e.g., alkalinity in Monte Romero was around 100 mg/L as $CaCO_3$, Caraballo et al., 2009) where no malachite was detected.

3.2. Evaluation of the long-term removal of different loads of sulfate using $BaCO_3$-DAS

The only previous experience using witherite to remove SO_4^{2-} from AMD waters reported very promising results, showing an almost complete SO_4^{2-} water removal after the treatment (Torres et al., 2018). However, it is important to notice the low water inflow and operation time of the experiment (Table 1), as well as the intermediate sulfate concentration of the water entering the $BaCO_3$-DAS column (i.e., from the 5000 mg/L of sulfate in the original AMD only 1,770 mg/L exits the $CaCO_3$-DAS column and enters the $BaCO_3$-DAS column). As a result, the $BaCO_3$-DAS column was submitted to a very modest sulfate load (0.7 g of SO_4^{2-} per day) on this experiment. To get a better understanding of the $BaCO_3$-DAS technology response when submitted to higher sulfate loads, the $BaCO_3$-DAS columns of the present study were designed to received 1.9 and 13.3 g/day of SO_4^{2-} (i.e., 2.7 and 19 times more sulfate than the experiment by Torres et al., 2018).

To facilitate the explanation of the main findings during these multiple experiments, the results from experiment B.1 (sulfate load of 1.9 g/day) will be used to exemplify the general geochemical performance of the $BaCO_3$-DAS columns. According to equation (1) the main expected effects of witherite dissolution should be an increase on water pH and a decrease on sulfate concentration. In addition, the waters may also exhibit a local increase in the concentration of barium (Ba, depending on the local final balance

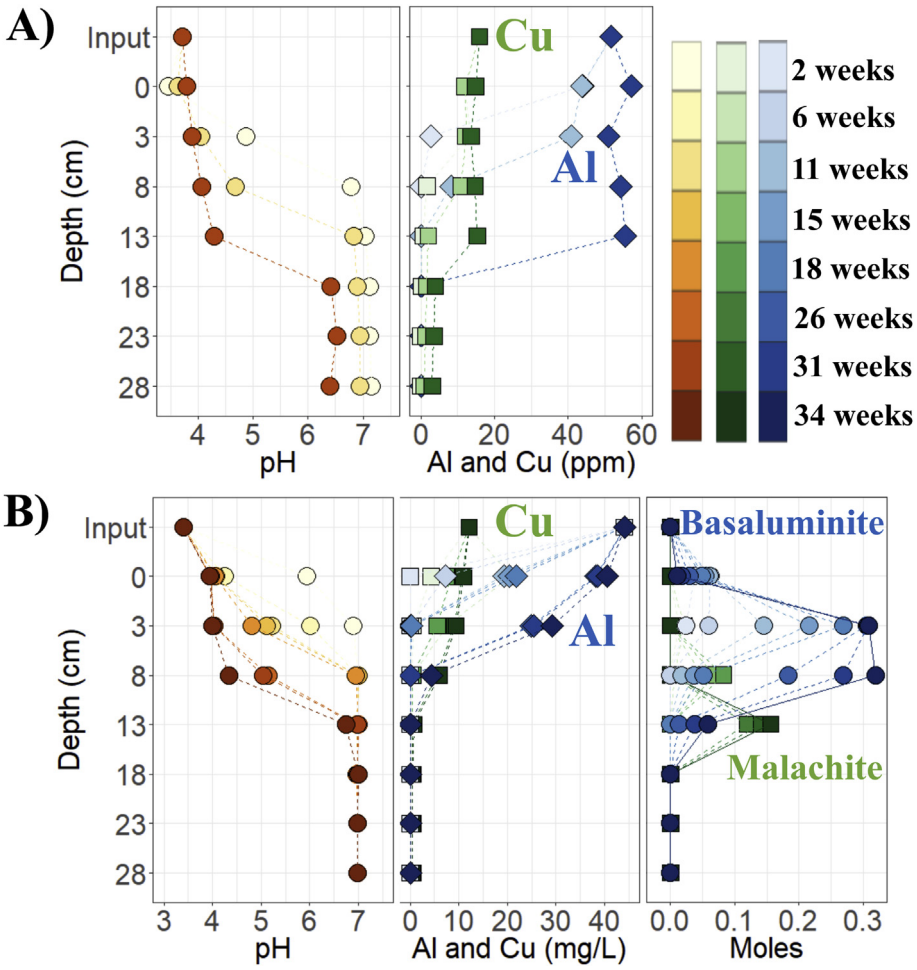

Fig. 2. All the results correspond to the mussel shell-DAS column at experiment B.2. A) Spatial and temporal evolution of some representative operational parameters along the column, and B) Results obtained in the geochemical model performed with Phreeqc.

between witherite dissolution and barite precipitation) as well as some local decrease in Ca concentration as a result of $CaCO_3$ precipitation. Taking into account all these processes, it can be inferred that the $BaCO_3$-DAS column on experiment B.1 showed signs of witherite dissolution during the first 6 months of operation (Fig. 4A). During this period, the water outflowing the column always showed sulfate concentrations lower than 500 mg/L. However, if the geochemistry time series of the column are observed in detail, it can be observed how after 17 weeks of operation the sulfate concentration began to increase as water pH and exceeding dissolved Ba starts to decrease upward from the bottom of the column (Fig. 4A). This peculiar behavior cannot be explained by witherite exhaustion. As shown in the hydrochemical model performed (Fig. 4B), if the column would have progressively consumed the available witherite downward the column (as it did for the $CaCO_3$-DAS columns and during the early weeks of the $BaCO_3$-DAS experiments), it should have shown better sulfate removal and more steady water pHs (between 8 and 9) along the 38 weeks of the experiments.

Also, it is important to notice that this evolution of the hydrochemical depth profiles is much faster in the $BaCO_3$-DAS column at experiment B.2 (Figure A.9.B, Appendix). Because of the higher sulfate load received by this column (13.3 g/day), the first signs of the reactive material exhaustion were observed after 11 weeks of operation and the remediation capacity of the column completely stopped after 18 weeks of operation. In addition, these figures show how both $BaCO_3$-DAS columns achieved an excellent Mn removal when witherite dissolution is actively occurring. Therefore, by using witherite the need of a MgO-DAS step to remove divalent metals (like Mn^{2+}) could be avoided.

To obtain a different perspective helping to explain the geochemical evolution of the column, several solid samples at different depths within the column were obtained and studied by XRD. During this solid sampling campaign, a visual inspection of the two $BaCO_3$-DAS columns allowed identifying two well differentiated vertical zones. The first zone (wall zone) corresponded to the reactive material close to the wall in contact with the inflowing water (notice that the design of the column induced that the inflowing water run down the wall of the column instead of directly dripping to the supernatant of the column, Figure A.10). The second zone (core zone) corresponded to most of the column and it is characterized by a less cemented less compacted material (if compared with the samples from the wall zone). The semi-quantitative mineralogical characterization of these samples are shown in Table 4. As it can be observed, all the columns and sections are characterized by and almost complete or complete exhaustion of the original witherite as well as by the significant precipitation of $CaCO_3$ mineral phases (i.e., calcite and/or aragonite) and barite (Fig. A4 and A.5, Appendix). Both $BaCO_3$-DAS columns typically show higher amounts of $CaCO_3$ precipitates (calcite + aragonite) in the samples from the wall section (if compared with the sample from the core section). These results are

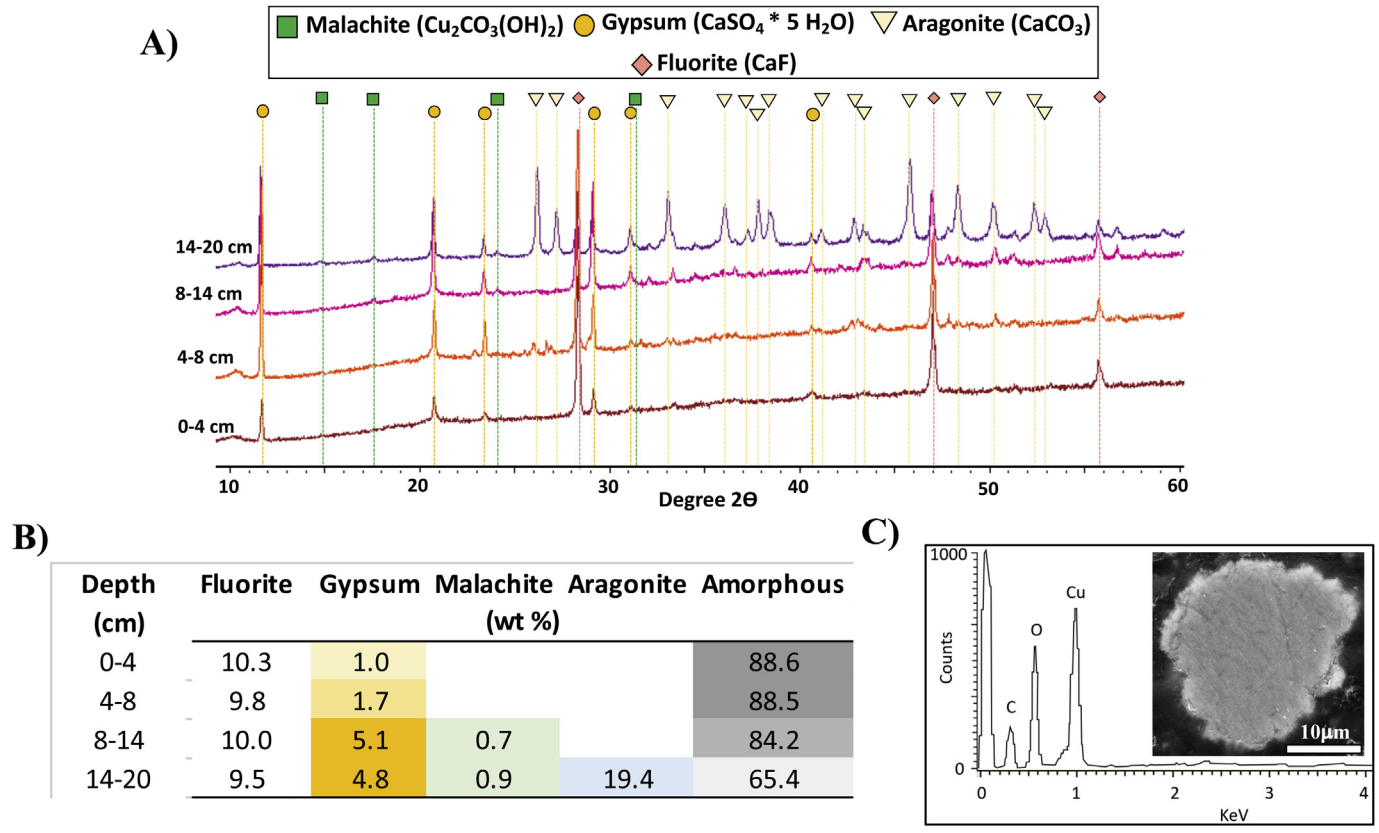

Depth (cm)	Fluorite	Gypsum	Malachite	Aragonite	Amorphous
	(wt %)				
0-4	10.3	1.0			88.6
4-8	9.8	1.7			88.5
8-14	10.0	5.1	0.7		84.2
14-20	9.5	4.8	0.9	19.4	65.4

Fig. 3. Mineralogical and chemical evidences of the presence of malachite within mussel shell-DAS column at experiment B.2. A) Stacked X-Ray diffractograms and mineral peaks assignment; B) Mineral semi-quantification using fluorite as internal standard; and C) EDS pattern and SEM electron backscattered image of a malachite single particle.

in accordance with the visual observations during the sampling and could explain the higher cementation of the samples from the wall section. It is also important to notice that the $BaCO_3$-DAS column at experiment B.2 showed no signs of witherite in the wall section whereas some remaining witherite was detected in the samples from the core section.

Another independent observation that could help explaining the geochemical behavior of the columns, is that during the columns operations they did not show any clogging problem (i.e., the inflow rate was kept constant and the water supernatant did not need to increase its hydraulic head to maintain the same outflow rate), despite the important mineral precipitation within the columns. In addition, a different coloring of the reactive material within the columns was developed during the experiment. At the end of the experiment, it was possible to clearly differentiate the wall and core sections within the column (the wall section went darker whereas the core section maintained the original coloring of the reactive mixture).

Considering all these independent observations, the following plausible interpretation for the column geochemical behavior and evolution is offered: During the first months of operation (i.e., 24 and 11 weeks at experiment B.1 and B.2, respectively) the $BaCO_3$-DAS columns showed signs of witherite dissolution and accomplished sulfate output concentrations lower than 500 mg/L. However, these columns began to exhibit the effect of preferential flows and water mixing a few weeks earlier. As a result, from the sixth (B.1) and fourth (B.2) months to the last of the experiments the columns lost their remediation capacities, but they maintained their original hydraulic conductivity due to the generation of preferential flow paths.

Moreover, the experimental design allowed gaining a better understanding of the $BaCO_3$-DAS technology regarding its sulfate removal efficiency and lifetime. The information is graphically presented on Fig. 5, but it is also shown *in extenso* in the Supplementary Information (Table S7). Comparing the results in Fig. 5, it can be observed how an increase in the sulfate load received by the columns implied a decrease in their lifetime (i.e., moment when the water outflowing the column reach a value higher than 500 mg/L, yellow circles on the figure). On the other hand, the $BaCO_3$-DAS column in experiment B.2 was able to achieve a higher accumulated removed sulfate load during its shorter operation time but it has to be considered that a double amount of witherite (i.e., 2 kg instead of 1 kg) was used on this experiment.

4. Conclusions, implications and future challenges

The present study has shown how other sources of $CaCO_3$ (i.e., mussel shells, clams shells and eggshells) might be as efficient (or even more) than limestone to remove Fe, Al and Cu from AMD polluted waters. These observations could facilitate the improvement of the DAS technology environmental footprint by reusing alternative by-product or residues (instead of mining raw materials) from local industries closer to the future full-scale treatment locations. However, to really consider these replacement alkaline reagents as more sustainable options than limestone, it is always necessary to perform a Life Cycle Assessment (LCA) including the whole context of the specific site where a passive treatment could be implemented.

It is also important to notice that, for the first time, malachite has been confirmed as a mineral actively involved in the AMD remediation processes. This observation is of a great importance for the optimum implementation of the DAS technology in AMDs with

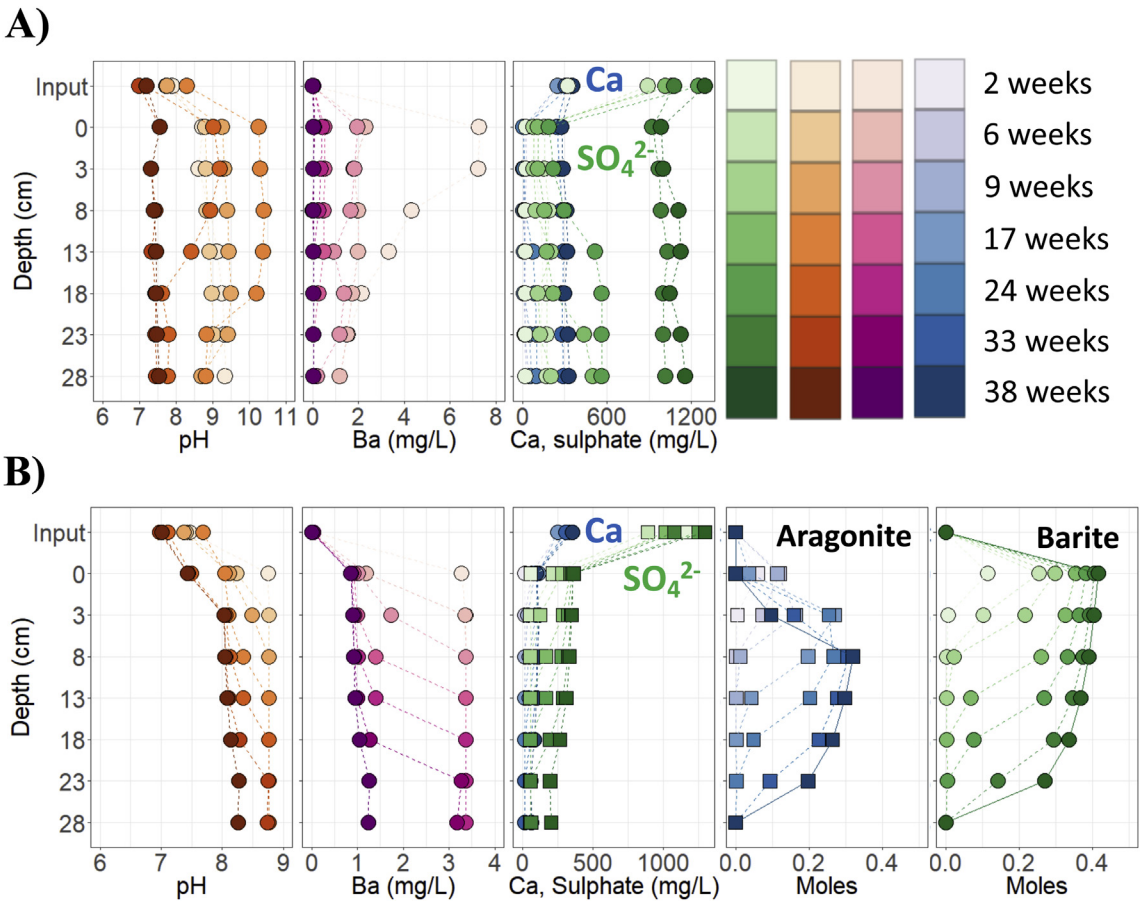

Fig. 4. Raw (A) and modeled (B) hydrochemical depth profiles of the main operational parameters and elements within the $BaCO_3$-DAS column in experiment B.1. Notice that modeled precipitation profiles of barite ($BaSO_4$) and aragonite ($CaCO_3$) are shown in B), where positive values correspond to precipitated amount of mineral.

Table 4
Mineralogical identification and semi-qualification of selected samples along the depth profile of the BaCO3-DAS columns in experiments B.1 and B.2.

Experiment	Depth (cm)	Fluorite	Barite	Calcite	Aragonite	∑$CaCO_3$	Witherite	Amorphous
		(wt %)						
B.1	0-4	10.0	5.5		1.4	1.4	2.4	80.7
	4-8	9.5	1.2		4.0	4.0	1.1	84.3
	13-18	10.2	1.1		4.1	4.1		84.5
B.1_Wall	0-4	10.6	2.3		10.8	10.8	2.3	74.0
	4-8	10.8	1.8		8.7	8.7	3.8	74.9
	13-18	10.3	1.2		2.8	2.8	1.9	83.9
B.2	0-4	9.7	0.8	1.0	1.8	2.8	2.4	88.6
	4-8	10.6	9.1		2.2	2.2	1.1	88.5
	13-18	10.7	13.0		3.1	3.1	1.0	84.2
	23-30	9.6	2.2	2.1		2.1	2.7	65.4
B.2_Wall	0-4	10.9	5.2	0.7	0.5	1.2		84.2
	4-8	10.2	6.3	0.7	1.0	1.8		76.9
	13-18	9.6	1.5	2.0	4.2	6.1		72.2
	23-30	9.6	2.9	3.9		3.9		83.3

∑$CaCO_3$ = addition of calcite and aragonite concentrations (wt %). B.1 and B.2 correspond to samples obtained from the core of the column, whereas samples B.1_Wall and B.2_Wall were obtained close to the wall of the columns.

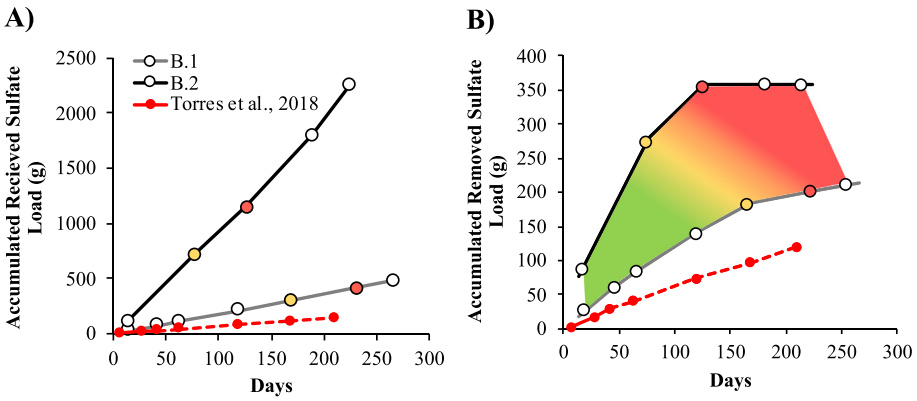

Fig. 5. A) Accumulated received sulfate load and B) accumulated removed sulfate load in the two tested $BaCO_3$-DAS columns (i.e., B.1 and B.2) and the experiment by Torres et al. (2018). The circles colored in yellow and red mark the moments when the output sulfate concentrations reached values higher than 500 mg/L and 1000 mg/L, respectively. The dotted line in Torres et al. (2018) correspond to modeled data. (For interpretation of the references to color in this figure legend, the reader is referred to the Web version of this article.)

low to medium metal contents, because the mineralogical/geochemical reactions involved in the remediation process may be more diverse than previously thought. Also, it is important to notice that malachite stability highly depends on water pH (malachite equilibrium pH is around 7, depending on the water chemistry). Therefore, if a low-pH front migrates down the treatment system (as calcite is exhausted through the months) malachite will be unstable and it will become a pollution source. Something similar to what has been reported for hydrobasaluminite (equilibrium pH of 4.5). Consequently, it was confirmed that the implementation of a DAS-type technology is not straightforward, not only because the few operational parameters that have to be optimized and its working ranges defined (i.e., residence time, flowrate that can be treated or the reagent useful lifetime) but also because of new geochemical and mineralogical reaction that may be involved depending on the precise elemental composition and elemental ratio of the AMD to be treated.

Taking into consideration present and previous results, the $BaCO_3$-DAS reagent lifetime clearly depends on the sulfate load entering the system (i.e., higher sulfate loads = lower lifetime of the reagent material; Fig. 5). Despite the observed generation of preferential flow paths within the $BaCO_3$-DAS columns, most of the available witherite was completely or almost completely consumed in the different sections of the columns (Table 4) achieving lifetimes of up to 6 months. Therefore, although further investigations are necessary to avoid undesired preferential flow paths within the reactive mixture, this optimization is not expected to significantly extend the lifetime of the reactive mixture.

The guidance of previous experiences on upscaling DAS technology from laboratory-scale experiments to full scale field passive treatment systems was used on the present discussion. The reader is referred to previous works for more details about upscaling and field full-scale implementation of DAS technology (Ayora et al., 2013; Martínez et al., 2018). Nonetheless, it is worth to mention that the calculation of an even estimative cost for the full scale implementation of this technology is highly dependent on many site-specific factors, like: 1) water chemistry, 2) flowrate, 3) level of accessibility (or inaccessibility) of the construction site, 4) distance from the chemical reagent and construction suppliers bases to the construction site, and 5) cost of civil engineering works; just to mentioned a few. As a result, very different prices will arise for the implementation of this technology on two full scale treatments at two very different realities. Just to offer a made-up but realistic example, the reader can easily anticipate the very different costs for the final implementation a of a full-scale treatment system in 1) Chile (in a high mountainous inaccessible region with low acidity waters and low flowrate, for example) where just one or two reactive tanks and decantation ponds may be needed to restore the water quality, or 2) Spain (in a low mountainous accessible region with very high acidity waters and medium-low flowrate, for example) where at least three much bigger reactive pools and decantation ponds may be necessary. Building the first one (Capex) could be in the order of 500,000 US$ while the second could be in the order 1 to 2 million euros. The Opex of these made-up treatments would show even more differences between them because the reagents consumption and treatment residues management (main Opex costs) are highly variable depending on the metallic and sulfate loads of the waters, and on the environmental legislation of each specific country.

To get a realistic estimate of the costs associated with the use of witherite as reagent material, the following upscaling exercise is offered. To begin with, the accumulated removed sulfate load per volume of reactive mixture at the end of the system optimal performance was calculated (Table A.6, Appendix). This parameter ranged between 0.035 and 0.053 g of SO_4^{2-}/cm^3 of $BaCO_3$-DAS. If it is assumed that the reactive mixture presents the same performance at field full-scale and AMDs with the same compositions of the present study have to be remediated, a 1000 m^3 reactive pool (20 m × 25 m x 2,5 m; length x width x depth) would be able to treat water inflows ranging from 3.3 to 11.8 L/s. This inflow rate is too low to remediate AMDs at active mine sites that typically exhibit flowrate of tens to hundreds of L/s. However, it perfectly fits the needs of abandoned and/or closed mine sites where the flow rates typically range between a few units to a few tens of L/s. Following this exercise and considering a cost of the commercial $BaCO_3$ reagent of 300 US$/t (https://www.alibaba.com/showroom/barium-carbonate-price.html), the cost of the needed $BaCO_3$ for the reactive pool treating 3.3 L/s of AMD would be around 50,000 US$. $BaCO_3$ current high price can be a serious obstacle for the economic feasibility of these type of passive treatment systems. However, several studies are setting the ground for the transformation of barite ($BaSO_4$) into witherite ($BaCO_3$) using a chemical engineering process based on the thermal reduction of $BaSO_4$ and $CaCO_3$ (combustion at 1050 °C in the presence of coal) transforming $BaSO_4$ into BaS. The bubbling of CO_2 in the resulting BaS aqueous slurry finally produce $BaCO_3$ and S (Masukume et al., 2013; Mulopo, 2015). Since the final residue of the $BaCO_3$-DAS treatment is rich in both barite and calcite, the regeneration of this material could be a

plausible option to improve the economic feasibility of the project under a circular economy perspective. The addition of a $BaCO_3$ regeneration process would affect both the OPEX and sustainability of the passive treatment, and a detail life cycle assessment of the specific final treatment configuration should be performed (to evaluate the feasibility of the new technological solution).

CRediT authorship contribution statement

Alfonso Larraguibel: Conceptualization, Formal analysis, Investigation, Methodology, Writing - original draft, Writing - review & editing. **Alvaro Navarrete-Calvo:** Formal analysis, Investigation, Methodology, Project administration, Writing - review & editing. **Sebastián García:** Investigation, Software, Writing - review & editing. **Víctor F. Armijos:** Funding acquisition, Project administration, Writing - review & editing. **Manuel A. Caraballo:** Conceptualization, Funding acquisition, Investigation, Methodology, Project administration, Writing - original draft, Writing - review & editing, Supervision.

Declaration of competing interest

None.

Acknowledgments

This study was funded by CORFO and Sacyr Chile through the project 16COTE-60128. It was also partially financed by the projects CONICYT/PIA Project AFB180004, FONDECYT Initiation Project 11150002 and FONDEQUIP (Project EQM130119). The authors thank Mario Jara for their analytical assistance. The authors thank Dr. Panos Seferlis (Associate Editor) and three anonymous reviewers for their suggestions and comments that significantly improved the quality of the original manuscript.

Appendix A. Supplementary data

Supplementary data to this article can be found online at https://doi.org/10.1016/j.jclepro.2020.123450.

References

Akcil, A., Koldas, S., 2006. Acid Mine Drainage (AMD): causes, treatment and case studies. J. Clean. Prod. 14 (12–13), 1139–1145.

Ayora, C., Macías, Francisco, Torres, Ester, Lozano, Alba, Carrero, Sergio, Nieto, Jose-Miguel, Perez-Lopez, Rafael, Fernandez-Martínez, Alejandro, Castillo-Michel, Hiram, 2016. Recovery of rare earth elements and yttrium from passive-remediation systems of acid mine drainage. Environ. Sci. Technol. 50 (15), 8255–8262. https://doi.org/10.1021/acs.est.6b02084. In press.

Ayora, C., Caraballo, M.A., Macias, F., Rötting, T.S., Carrera, J., Nieto, J.M., 2013. Acid mine drainage in the Iberian Pyrite Belt: 2. Lessons learned from recent passive remediation experiences. Environ. Sci. Pollut. Control Ser. 20 (11), 7837–7853.

Barra, F., Reich, M., Selby, D., Rojas, P., Simon, A., Salazar, E., Palma, G., 2017. Unraveling the origin of the Andean IOCG clan: a Re-Os isotope approach. Ore Geol. Rev. 81, 62–78.

Bavandpour, F., Zou, Y., He, Y., Saeed, T., Sun, Y., Sun, G., 2018. Removal of dissolved metals in wetland columns filled with shell grits and plant biomass. Chem. Eng. J. 331, 234–241.

Camus, F., Dilles, J.H., 2001. A special issue devoted to porphyry copper deposits of northern Chile. Econ. Geol. 96 (2), 233–237.

Caraballo, M.A., Rötting, T.S., Nieto, J.M., Ayora, C., 2009. Sequential extraction and DXRD applicability to poorly crystalline Fe-and Al-phase characterization from an acid mine water passive remediation system. Am. Mineral. 94 (7), 1029–1038.

Caraballo, M.A., Rötting, T.S., Silva, V., 2010. Implementation of an MgO-based metal removal step in the passive treatment system of Shilbottle, UK: Column experiments. J. Hazard. Mater. 181 (1–3), 923–930. https://doi.org/10.1016/j.jhazmat.2010.05.100. In press.

Caraballo, M.A., Macías, F., Nieto, J.M., Castillo, J., Quispe, D., Ayora, C., 2011. Hydrochemical performance and mineralogical evolution of a dispersed alkaline substrate (DAS) remediating the highly polluted acid mine drainage in the full-scale passive treatment of Mina Esperanza (SW Spain). Am. Mineral. 96 (8–9), 1270–1277.

Delgado, J., Barba-Brioso, C., Ayala, D., Boski, T., Torres, S., Calderon, E., Lopez, F., 2019. Remediation experiment of Ecuadorian acid mine drainage: geochemical models of dissolved species and secondary minerals saturation. Environ. Sci. Pollut. Control Ser. 26, 34854–34872. https://doi.org/10.1007/s11356-019-06539-3.

Dold, B., 2014. Evolution of acid mine drainage formation in sulphidic mine tailings. Minerals 4 (3), 621–641.

FAO, 2018. Global Aquaculture Production 1950-2016 Database. Available at. http://www.fao.org/fishery/statistics/global-aquaculture-production/query/es.

Gazea, B., Adam, K., Kontopoulos, A., 1996. A review of passive systems for the treatment of acid mine drainage. Miner. Eng. 9 (1), 23–42.

INAP, 2003. Treatment of sulfate in mine effluents. In: International Network for Acid Prevention. LORAX Environmental Inc. October, 2003. Retrieved from. http://www.inap.com.au/public_downloads/Research_Projects/Treatment_of_Sulphate_in_Mine_Effluents_-_Lorax_Report.pdf.

Jacobs, J.A., Lehr, J.H., Testa, S.M., 2014. Acid Mine Drainage, Rock Drainage, and Acid Sulfate Soils: Causes, Assessment, Prediction, Prevention, and Remediation. John Wiley & Sons.

Johnson, D.B., Hallberg, K.B., 2005. Acid mine drainage remediation options: a review. Sci. Total Environ. 338 (1–2), 3–14.

Kefeni, K.K., Msagati, T.A., Mamba, B.B., 2017. Acid mine drainage: prevention, treatment options, and resource recovery: a review. J. Clean. Prod. 151, 475–493.

Macías, F., Caraballo, M.A., Rötting, T.S., Pérez-López, R., Nieto, J.M., Ayora, C., 2012. From highly polluted Zn-rich acid mine drainage to non-metallic waters: implementation of a multi-step alkaline passive treatment system to remediate metal pollution. Sci. Total Environ. 433, 323–330.

Martinez-Garcia, C., Gonzalez-Fonteboa, B., Martinez-Abella, F., Carro- Lopez, D., 2017. Performance of mussel shell as aggregate in plain concrete. Construct. Build. Mater. 139, 570–583.

Martínez, N.M., Basallote, M.D., Meyer, A., Cánovas, C.R., Macías, F., Schneider, P., 2018. Life cycle assessment of a passive remediation system for acid mine drainage: towards more sustainable mining activity. J. Clean. Prod. 211, 1100–1111.

Martinez-Garcia, C., Gonzalez-Fonteboa, B., Carro-Lopez, D., Martinez-Abella, F., 2019. 8 - recycled mollusc shells, editor(s): jorge de Brito, francisco Agrela. In: Woodhead Publishing Series in Civil and Structural Engineering, New Trends in Eco-Efficient and Recycled Concrete. Woodhead Publishing, ISBN 9780081024805, pp. 191–205. https://doi.org/10.1016/B978-0-08-102480-5.00008-7.

Masukume, M., Maree, J.P., Ruto, S., Joubert, H., 2013. Processing of barium sulphide to barium carbonate and sulphur. Chem. Eng. Proc. Technol. 4, 157. https://doi.org/10.4172/2157-7048.1000157.

Mulopo, J., 2015. Continuous pilot scale assessment of the alkaline barium calcium desalination process for acid mine drainage treatment. J. Environ. Chem. Eng. 3, 1298–1302.

Parkhurst, D.L., Appelo, C.A.J., 2013. Description of input and examples for PHREEQC version 3—A computer program for speciation, batch-reaction, one-dimensional transport, and inverse geochemical calculations. U.S. Geological Survey Techniques and Methods book 6, chap. A43, 497 p., available only at. https://pubs.usgs.gov/tm/06/a43/.

Rose, A.W., Bisko, D., Daniel, A., Bower, M.A., Heckman, S., 2004. An “autopsy” of the failed Tangaskootack #1 vertical fl ow pond, Clinton Co., Pennsylvania. p. 1580–1594. In: Barnhisel, R.I. (Ed.), Joint Conference of the 21st Annual Meetings of the American Society of Mining and Reclamation and 25th West Virginia Surface Mine Drainage Task Force Symposium, Morgantown, WV. ASMR, Lexington, KY.

Rötting, T.S., Thomas, R.C., Ayora, C., Carrera, J., 2006a. Challenges of passive treatment of metal mine drainage in the Iberian Pyrite Belt (Southern Spain): preliminary studies. In: Proc. Of the Seventh Int. Conf. on Acid Rock Drainage, pp. 1753–1767. St. Louis, MO.

Rötting, T.S., Caraballo, M.A., Serrano, J.A., Ayora, C., Carrera, J., 2008a. Field application of calcite Dispersed Alkaline Substrate (calcite-DAS) for passive treatment of acid mine drainage with high Al and metal concentrations. Appl. Geochem. 23 (6), 1660–1674. https://doi.org/10.1016/j.apgeochem.2008.02.023.

Rötting, T.S., Thomas, R.C., Ayora, C., Carrera, J., 2008b. Passive treatment of acid mine drainage with high metal concentrations using dispersed alkaline substrate. J. Environ. Qual. 37 (5), 1741–1751. https://doi.org/10.2134/jeq2007.0517.

Rötting, T.S., Cama, J., Ayora, C., Cortina, J.L., De Pablo, J., 2006b. Use of caustic magnesia to remove cadmium, nickel, and cobalt from water in passive treatment systems: column experiments. Environ. Sci. Technol. 40 (20), 6438–6443.

Rakotonimaro, T.V., Neculita, C.M., Bussière, B., Zagury, G.J., 2016. Effectiveness of various dispersed alkaline substrates for the pretreatment of ferriferous acid mine drainage. Appl. Geochem. 73, 13–23.

Rakotonimaro, T.V., Neculita, C.M., Bussière, Genty, T.B., Zagury, G.J., 2018. Performance assessment of laboratory and field-scale multi-step passive treatment of iron-rich acid mine drainage for design improvement. Environ. Sci. Pollut. Control Ser. 25, 17575–17589. https://doi.org/10.1007/s11356-018-1820-x.

Sheoran, A.S., Sheoran, V., 2006. Heavy metal removal mechanism of acid mine drainage in wetlands: a critical review. Miner. Eng. 19 (2), 105–116.

Simón, M., Martín, F., García, I., Bouza, P., Dorronsoro, C., Aguilar, J., 2005. Interaction of limestone grains and acidic solutions from the oxidation of pyrite tailings. Environ. Pollut. 135 (1), 65–72.

Skousen, J., Ziemkiewicz, P., 2005. Performance of 116 passive treatment systems for

acid mine drainage. In: Proceedings, American Society of Mining and Reclamation, pp. 1100–1133. Breckenridge, CO.
Skousen, J., Zipper, C.E., Rose, A., Ziemkiewicz, P.F., Nairn, R., McDonald, L.M., Kleinmann, R.L., 2017. Review of passive systems for acid mine drainage treatment. Mine Water Environ. 36 (1), 133–153.
Torres, E., Lozano, A., Macías, F., Gomez-Arias, A., Castillo, J., Ayora, C., 2018. Passive elimination of sulfate and metals from acid mine drainage using combined limestone and barium carbonate systems. J. Clean. Prod. 182, 114–123.
USEPA. U.S. Environmental Protection Agency, 2017. National drinking water regulations. Retrieved from. https://www.epa.gov/dwstandardsregulations.
Valenzuela, M., 2019. MsCminingthesis *"Monitoreo ambiental y análisis espacio temporal de la calidad hídrica de la cuenca del Mapocho"*. Graduated. Universidad de Chile, Santiago.
WHO, World Health Organization, 2008. Guidelines for Drinking-Water Quality, fourth ed. Retrieved from. http://www.who.int/water_sanitation_health/dwq/fulltext.pdf.
Younger, P.L., Banwart, S.A., Hedin, R.S., 2002. Mine Water: Hydrology, Pollution, Remediation. Kluwer, Dordrecht, p. 442.
Younger, P.L., Wolkersdorfer, C., 2004. Mining impacts on the fresh water environment: technical and managerial guidelines for catchment scale management. Mine Water Environ. 23, s2–s80.
Ziemkiewicz, P.F., Skousen, J.G., Simmons, J., 2003. Long-term performance of passive acid mine drainage treatment systems. Mine Water Environ. 22, 118–129.